



## OPEN ACCESS

## EDITED BY

Mingliang Tian,  
Hefei Institutes of Physical Science  
(CAS), China

## REVIEWED BY

Deepak K. Pandey,  
KICVentures Group - The LES Institute,  
United States  
Xue Liu,  
Anhui University, China

## \*CORRESPONDENCE

David Carroll,  
carrolld@wfu.edu

## SPECIALTY SECTION

This article was submitted to Quantum  
Materials, a section of the journal  
Frontiers in Materials

RECEIVED 07 June 2022

ACCEPTED 03 October 2022

PUBLISHED 20 October 2022

## CITATION

Link R, Marcus G and Carroll D (2022),  
Solvothermal growth of moiré  
superlattices in antimony telluride  
spiral-type nanoplates.  
*Front. Mater.* 9:963775.  
doi: 10.3389/fmats.2022.963775

## COPYRIGHT

© 2022 Link, Marcus and Carroll. This is  
an open-access article distributed  
under the terms of the [Creative  
Commons Attribution License \(CC BY\)](#).  
The use, distribution or reproduction in  
other forums is permitted, provided the  
original author(s) and the copyright  
owner(s) are credited and that the  
original publication in this journal is  
cited, in accordance with accepted  
academic practice. No use, distribution  
or reproduction is permitted which does  
not comply with these terms.

# Solvothermal growth of moiré superlattices in antimony telluride spiral-type nanoplates

Robert Link, Gabriel Marcus and David Carroll\*

Center for Nanotechnology and Molecular Materials, Department of Physics, Wake Forest University, Winston-Salem, NC, United States

The study of moiré superlattices (MSLs) has surged in recent years, as they have been found to host several emergent quantum phenomena associated with high electron correlations. In this study, we put forward a viable chemical route to the formation of moiré patterns in antimony telluride ( $\text{Sb}_2\text{Te}_3$ ) nanoplates by leveraging screw dislocation-driven growth. These  $\text{Sb}_2\text{Te}_3$  MSLs are synthesized using a scalable, one-pot, colloidal solution-liquid-solid (SLS) procedure. We report twist angles up to  $0.52^\circ$  (estimated using a combination of transmission electron microscope (TEM) image analysis and computer simulation). We investigate the early growth stages of  $\text{Sb}_2\text{Te}_3$  spiral-type nanoplates under TEM, and we detail the growth of  $\text{Sb}_2\text{Te}_3$  spiral-type nanoplates that feature a central nanopore, caused by tandem growth with nanorods. We hope that these methods will facilitate future investigation into the electronic properties of  $\text{Sb}_2\text{Te}_3$  MSLs.

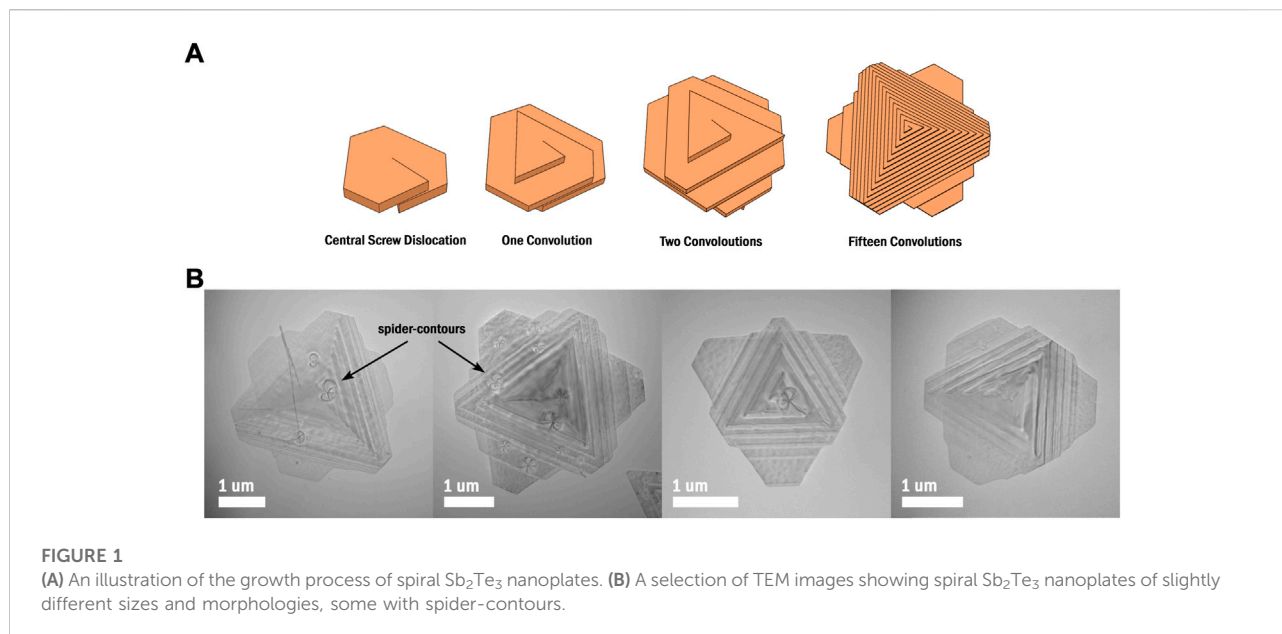
## KEYWORDS

moiré pattern, chalcogenide, topological insulator, quantum material, one pot synthesis, twistrionics, screw dislocation, van der waals materials

## 1 Introduction

Moiré superlattices (MSLs) are created when two or more heterogeneous or homogeneous atomically thin layers of van der Waals (vdW) material are stacked with a relative twist angle, creating periodic long-range changes in stacking order (Cao, Fatemi, Demir, et al., 2018; Liu et al., 2019). Since the discovery of superconducting and correlated insulating phases in “magic angle” twisted bilayer graphene, MSLs have become a central focus of materials research, spawning the new and promising subfield of twistrionics (Cao, Fatemi, Demir, et al., 2018; Cao, Fatemi, Fang, et al., 2018). MSLs of several 2D vdW materials have since been fabricated and studied, notably uncovering Wigner crystal states and provisional evidence for other highly correlated behaviors such as nematicity, quantum anomalous Hall and quantum spin Hall states, ferromagnetism, and superconductivity in transition metal dichalcogenide heterobilayers (Hennighausen et al., 2019; Li et al., 2021; Lau et al., 2022).

One key challenge that persists within the development of this research is the difficulty of fabricating MSLs, especially small twist angle MSLs. MSLs are commonly prepared using a process called the vdW transfer method. This method typically involves exfoliating a monolayer of vdW material, non-destructively transferring it onto a silicon substrate,



lifting a portion of that monolayer off of the substrate with a polymer stamp layered with hexagonal boron nitride, adjusting the angle of the substrate, and then lifting the remaining portion of monolayer off of the substrate and onto the polymer stamp (He et al., 2021). This process does allow for careful control of the resulting twist angle between layers; however, it is not a simple or particularly scalable process.

While many vdW materials can be formed into MSLs, the literature is primarily focused on bilayer graphene. In fact, graphene's often favorable properties as a conductor can render it unsuitable for applications in nanoelectronic devices that require a band gap. Thus, recent research has moved towards studying the properties of MSLs formed from semiconducting vdW materials. Among other class V-VI semiconductors, antimony telluride ( $\text{Sb}_2\text{Te}_3$ ) has garnered significant attention for its large thermoelectric effect; for its properties as a topological insulator; and for its layered structure, held together by vdW interaction. Numerous synthesis methods exist for  $\text{Sb}_2\text{Te}_3$  and similar chalcogenides, including chemical vapor deposition, exfoliation, and molecular-beam epitaxy. Colloidal solution-liquid-solid (SLS) chemistry is another method that can achieve effective synthesis of  $\text{Sb}_2\text{Te}_3$  and offers several significant advantages when compared to other methods. First, the synthesis set-up is inexpensive and does not require specialized laboratory equipment. Second, the reactions and associated steps required are straightforward and provide high purity yield of product. Third, SLS chemistry is highly versatile; by using one general procedure, a researcher can produce a wide array of materials and subsequently achieve edge modulation doping (Dun et al., 2017). Lastly, and perhaps the most important benefit of this approach, is that tweaking several reaction parameters can lead to a variety of morphological and structural changes in the final

material. A striking example of such a change is screw dislocation-driven growth in nanoplates, wherein the presence of a screw dislocation creates a 3D spiral structure instead of a simple 2D nanoplate. This growth pattern is general and has been observed in a wide range of materials including such vdW materials as SnSe,  $\text{WSe}_2$ , BiOCl,  $\text{Bi}_2\text{Se}_3$ , and  $\text{Sb}_2\text{Te}_3$  (Morin et al., 2011; Chen et al., 2014; Zhuang et al., 2014; Liu et al., 2016, 2019; Dun et al., 2017). Interestingly, in each of these cases, vdW gaps are located between the steps formed during dislocation-driven growth (Figure 1A). In the case of BiOCl, this structure has been leveraged to grow spiral nanosheets with a moiré pattern (Liu et al., 2019).

Growth of spiral  $\text{Sb}_2\text{Te}_3$  nanoplates by SLS method was first achieved in a recent paper by Dun et al. (2017), which serves as a foundational work for this study. In their paper, Dun et al. not only grew these topologically complex nanoplates, but further used the dangling tellurium bonds on the active nanoplate edges as heterogeneous nucleation sites, growing small silver (Ag) nanoparticles. The resulting Ag-decorated spiral nanoplates were then used to construct flexible thermoelectric thin films that remarkably saw a decoupled electrical conductivity and Seebeck effect. These thin films were measured to have a power factor of  $371 \mu\text{W m}^{-1} \text{K}^{-2}$  and a figure of merit ZT of 0.23.

The present study further develops the synthesis procedure put forth by Dun et al. (2017) in order to produce  $\text{Sb}_2\text{Te}_3$  spiral nanoplate MSLs. We additionally detail a procedure that produces spiral nanoplates with a central nanopore, caused by tandem growth with nanorods. Emphasis is given to modifications of the typical reaction procedure that lead to visible and controllable changes in the resulting nanocrystals. The crystal growth process and conditions necessary for the screw dislocation-driven growth of  $\text{Sb}_2\text{Te}_3$  are also explored in this

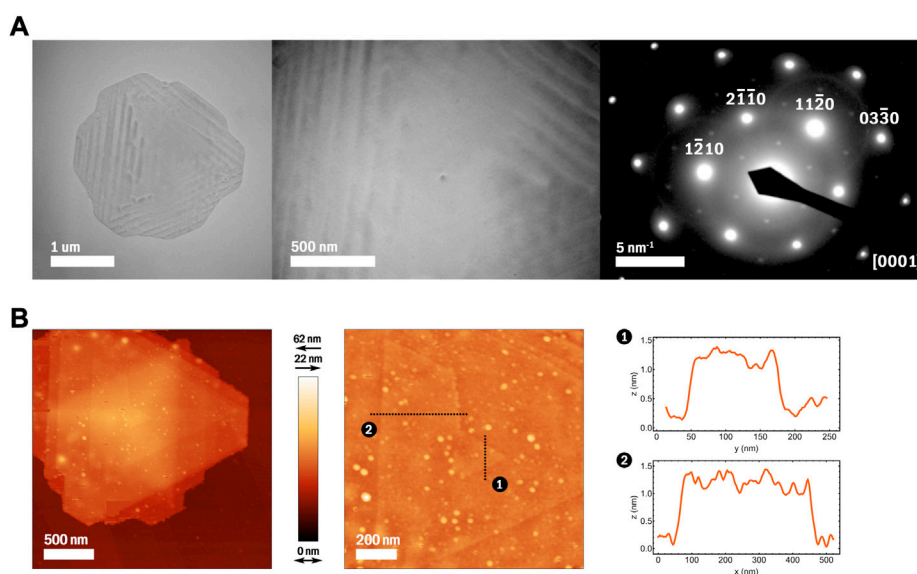


FIGURE 2

(A) TEM images and corresponding SAED pattern of an  $\text{Sb}_2\text{Te}_3$  spiral nanoplate with a visible core. (B) AFM images and height profile plots of an  $\text{Sb}_2\text{Te}_3$  spiral nanoplate showing the crystal steps to be 1 nm thick.

study. We propose that further research could yield a synthesis procedure for  $\text{Sb}_2\text{Te}_3$  MSLs with a twist angle that is controlled by tuning reaction parameters. Such a development could allow large scale production of  $\text{Sb}_2\text{Te}_3$  MSLs, ready for use in electronic systems.

## 2 Materials and methods

### 2.1 Synthesis of $\text{Sb}_2\text{Te}_3$ spiral-type nanoplates

The reaction that creates  $\text{Sb}_2\text{Te}_3$  spiral-type nanoplates (Figure 1B and Figure 2) takes place in one three-necked flask under reflux. Reactants 9 mmol of tellurium oxide ( $\text{TeO}$ ), 6 mmol of antimony chloride ( $\text{SbCl}_3$ ), 1.46 g of sodium hydroxide ( $\text{NaOH}$ ), and 800 mg of Polyvinylpyrrolidone (PVP) are dissolved into 70 ml of ethylene glycol (EG) one by one. Air is evacuated from the flask and replaced with argon gas. The flask is heated with a heating mantle to  $130^\circ\text{C}$  and held at this temperature for 10 min. In this time, the solution should turn black. Then, 8 ml hydrazine hydrate ( $\text{N}_2\text{H}_4$ ) is pumped into the flask at a pace of 2.5 ml per minute. The solution is then left to stir at  $130^\circ\text{C}$  for 3 hours before it is further heated to  $160^\circ\text{C}$  and left for an additional 15 h. In this time, the solution should lighten a bit to an opaque gray. Heating is then stopped, and the flask is left to cool.

At this stage, the nanoplates have formed and are well-coated with PVP, much of which must be washed away for successful edge doping, imaging, or other applications. Once the flask is

cool, the solution is divided into four centrifuge tubes. These tubes are then filled with acetone, and the nanoplates are collected into pellets by centrifugation at 5000 rpm for 20 min. The supernatant is discarded, after which the pellets are dispersed into 20 ml of ethanol by crushing with a glass stir rod, by vortexing, and by bath sonicating in water. This process is repeated by again by filling the tubes with acetone, followed by centrifugation. In this manner, the nanoplates are washed three to six times.

### 2.2 Synthesis of hexagonal $\text{Sb}_2\text{Te}_3$ nanoplates

The reaction that creates hexagonal  $\text{Sb}_2\text{Te}_3$  nanoplates (Figure 3) is identical to that of Section 2.1 with one exception. The 8 ml of  $\text{N}_2\text{H}_4$  is added at a rapid, unregulated pace before heating begins.

### 2.3 Synthesis of $\text{Sb}_2\text{Te}_3$ spiral-type nanoplates with moiré patterns

The reaction that creates  $\text{Sb}_2\text{Te}_3$  spiral-type nanoplates with moiré patterns (Figure 4) uses two three-necked flasks, joined with a distillation adapter. One flask is placed under reflux (Flask A). In Flask A, the same reactants as listed in Section 2.1 are dissolved into 70 ml of EG. An additional 1.5 ml of EG is placed in the remaining flask (Flask B). Air is then evacuated from the

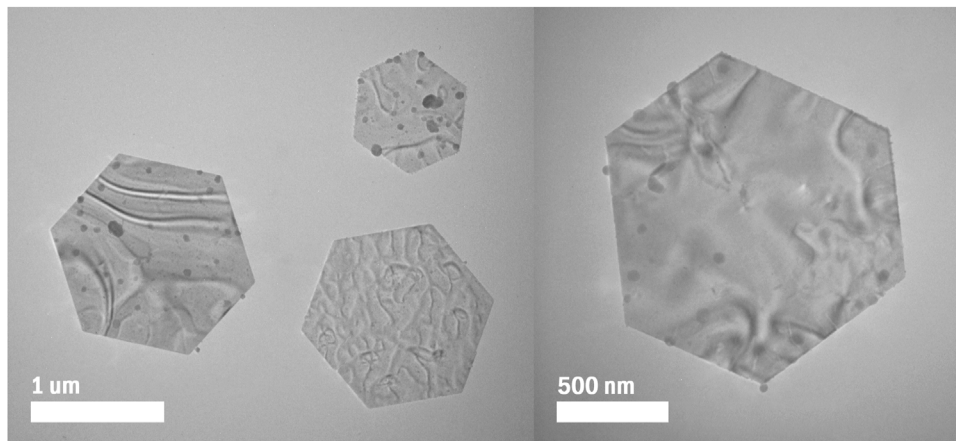


**FIGURE 3**  
TEM images of flat, hexagonal  $\text{Sb}_2\text{Te}_3$  nanoplates.

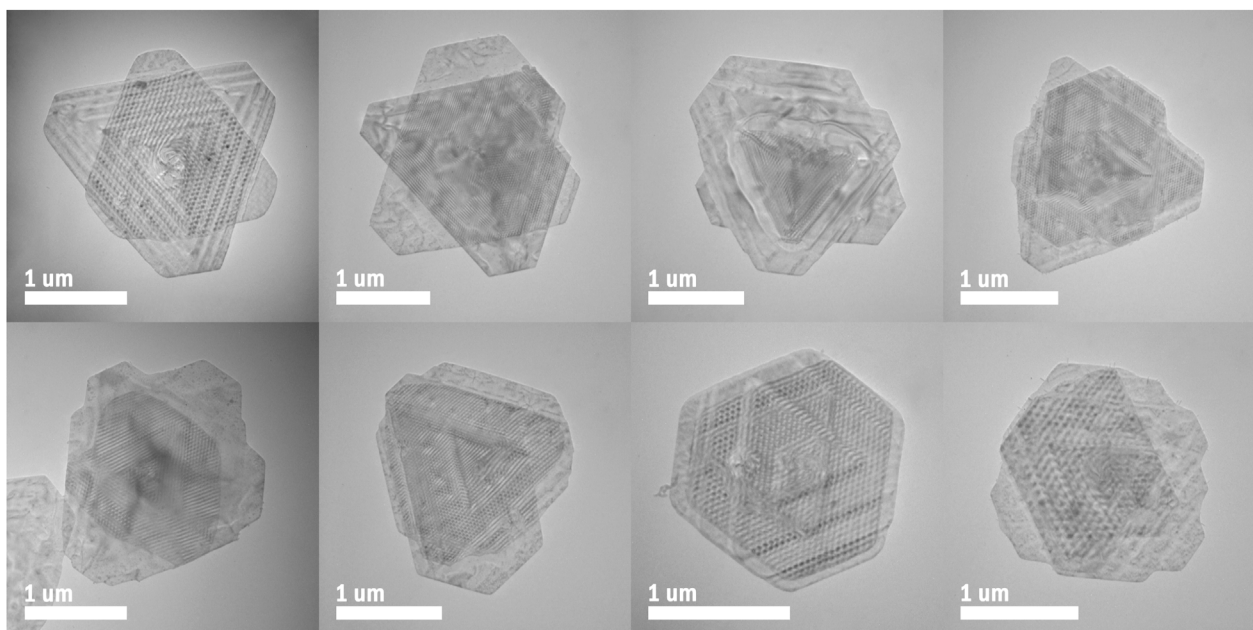


**FIGURE 4**  
TEM images of  $\text{Sb}_2\text{Te}_3$  spiral nanoplates, each with a visible moiré pattern.

setup and replaced with argon gas. Both flasks are heated simultaneously to  $130^\circ\text{C}$ . Then, 8 ml of  $\text{N}_2\text{H}_4$  is pumped into Flask B, such that it begins to vaporize and is slowly delivered as a vapor into Flask A. The solution is then left to stir at  $130^\circ\text{C}$  for 3 hours before it is further heated to  $160^\circ\text{C}$  and left for an additional 15 h. The heating is then stopped, the flasks are left to cool, and the resulting nanoplates are collected and washed as described in Section 2.1.

## 2.4 Synthesis of $\text{Sb}_2\text{Te}_3$ spiral-type nanoplates with central nanopores

The reaction that creates  $\text{Sb}_2\text{Te}_3$  spiral-type nanoplates with central nanopores (Supplementary Figure S1B) is identical to that of Section 2.3 with one exception. Into Flask B is added 30 ml of EG instead of 1.5 ml. This is done to further slow the rate of addition of  $\text{N}_2\text{H}_4$  into Flask A.



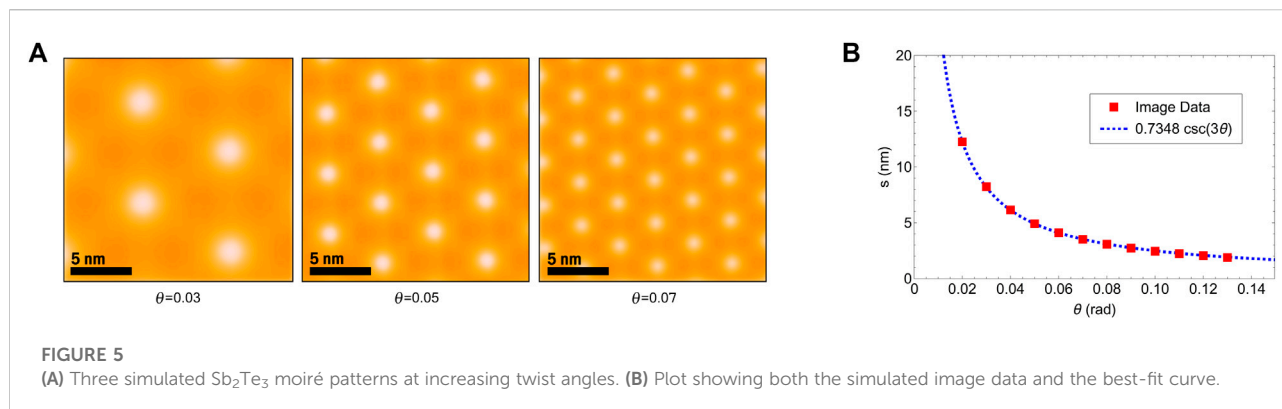


**FIGURE 5**  
(A) Three simulated  $\text{Sb}_2\text{Te}_3$  moiré patterns at increasing twist angles. (B) Plot showing both the simulated image data and the best-fit curve.

## 2.5 Sample characterization methods

Analysis of results from various reactions is performed by thorough examination of material sample images captured using a JEOL 1200-EX TEM equipped with a SIA-L3 camera. SAED analysis is also performed with the same machine. SAED image analysis was performed in CrysTBox. The AFM analysis in this study was performed by a Veeco Nanoscope IIIa Multimode in tapping mode. AFM image analysis was performed in Gwyddion. Moiré pattern simulation was performed by custom code written in Wolfram Mathematica, and TEM direct image analysis was performed using ImageJ.

## 3 Results and discussion

### 3.1 Spiral characterization results

Synthesized as described in Section 2.1; Figure 1B shows a selection of  $\text{Sb}_2\text{Te}_3$  spiral-type nanoplates. The growth of these nanoplates is driven by a central screw dislocation, causing the typically many-layered structure of  $\text{Sb}_2\text{Te}_3$  to instead form one continuous layer that spirals into a third dimension (Dun et al., 2017). Figure 1A illustrates how one screw dislocation is integral to this structural change. Given our colloidal synthesis method, and thus lack of substrate, the spiral-type nanoplates grow similarly on both sides, with a morphology like that of a trigonal bipyramid. Spider-contours are visible on many of these nanoplates (Figure 1B), often positioned at their center, which likely result from the strain field caused by screw dislocations (Morin et al., 2011). These nanoplates have been measured to range between  $4\mu\text{m}^2$  and  $10\mu\text{m}^2$  in area. Selected area electron diffraction (SAED) analysis of  $\text{Sb}_2\text{Te}_3$  spiral-type nanoplates (Figure 2A) reveals an interplanar spacing of 0.213 nm for planes  $(11\bar{2}0)$ ,  $(\bar{1}2\bar{1}0)$ , and  $(\bar{2}110)$ , while a spacing of 0.123 nm was measured for  $(03\bar{3}0)$ . These values match accepted values for  $\text{Sb}_2\text{Te}_3$  exactly to three decimal places. AFM analysis (Figure 2B) has revealed that the crystal steps of our spiral-type nanoplates are 1 nm in height, corresponding to one five-atom layer

of  $\text{Sb}_2\text{Te}_3$  (Dun et al., 2017). This supports the notion that our vdW gap is located between spiral steps. The total height of this sample was measured to be 25 nm (Supplementary Figure S1).

Careful and deliberate modification of synthesis procedures revealed that the quantity and rate of  $\text{N}_2\text{H}_4$  addition greatly impacts the morphology of the resulting nanomaterials. Without  $\text{N}_2\text{H}_4$ , only nanorods form. When  $\text{N}_2\text{H}_4$  is added with the other reactants, all at once before heating, screw dislocation-driven growth is not observed. Instead, flat hexagonal  $\text{Sb}_2\text{Te}_3$  nanoplates with a typical area of about  $1.5\mu\text{m}^2$  are formed (Figure 3). The slower addition of  $\text{N}_2\text{H}_4$  as a vapor, described in Section 2.3, frequently produces spiral nanoplates that exhibit moiré patterns (Figure 4). We propose that the presence of these patterns is due to increased strain within the central screw dislocation, resulting in a relative twist angle between spiral steps. While each spiral has many vdW gaps, observed moiré patterns are typically characteristic of a twist across only one gap, allowing interpretation of these patterns to be consistent with those produced by twisted bilayer  $\text{Sb}_2\text{Te}_3$ .

We performed a simulation in order to characterize the relationship between relative twist angle ( $\theta$ ) and moiré fringe spacing in bilayer  $\text{Sb}_2\text{Te}_3$ . A custom code was written that directly plots two lattices with a relative twist angle using graphics objects. Each lattice represents  $\text{Sb}_2\text{Te}_3$ 's five atomic sheet structure as seen from the  $[0001]$  zone axis. The scale of this plot is determined using the accepted values for the lattice constants of  $\text{Sb}_2\text{Te}_3$ . The resulting moiré pattern is then made more pronounced with careful use of uniform image filtering (Figure 5A). An isometric grid is fit to the set of brightest pixels within this plot, from which nearest neighbor spacing ( $s$ ) was measured. This process was repeated for several values of  $\theta$ , and from the resulting data was found the following best-fit equation with a root-mean-square error (RSME) of 0.032 nm (Figure 5B).

$$s = \left| \frac{0.7348}{\sin(3\theta)} \right|$$

With a choice of  $0 < \theta < \pi/6$ , this best-fit equation is easily inverted to estimate the twist angle of the  $\text{Sb}_2\text{Te}_3$  MSLs observed

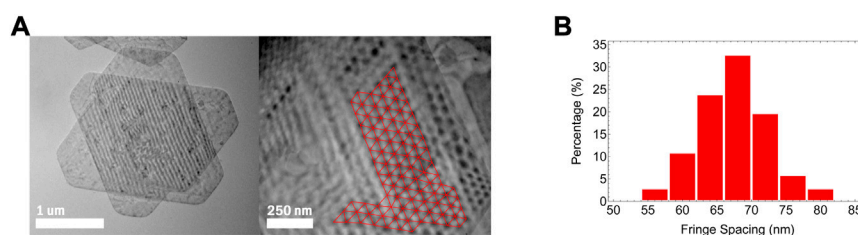


**FIGURE 6**

(A) TEM images of an  $\text{Sb}_2\text{Te}_3$  nanoplate with a visible moiré pattern. A nearest-neighbor grid is marked in red. (B) A histogram showing the distribution of side lengths in this nearest-neighbor grid. A fringe spacing of  $67.60 \pm 0.05$  nm is determined from this data, and thus an estimated twist angle of  $0.2074 \pm 0.0003^\circ$ .

with TEM. Moiré fringe spacing was measured from TEM images in agreement with our simulation: by fitting a nearest-neighbor grid to the dark spots of an MSL (Figure 6A). From this grid is produced a distribution of lengths (Figure 6B), from which is extracted an average value for  $s$  and its error. Using our equation obtained from simulation,  $\theta$  values are then estimated. Twenty MSLs were analyzed in this manner; between nanoplates,  $\theta$  values ranged from  $0.14^\circ$  to  $0.52^\circ$  and measurement error never exceeded 0.2%. Additional detail is provided in the [Supplementary Materials](#). Twist angles in vdW materials have also been effectively measured using SAED pattern analysis (Liu et al., 2019). In our case, the reported twist angles are too small to be properly quantified using this method (Supplementary Figure S6).

To observe the nanoplate growth process directly, samples were extracted from early stages of synthesis and examined with TEM. Minutes after heating begins, nanorods form in solution, turning the solution black. Nanoplates then nucleate and grow at the tips of these nanorods in the following few hours of heating (Supplementary Figure S4). Interestingly, this process is analogous to the vapor-phase snowflake growth performed by Libbrecht (2005), wherein the growth phases of ice were manipulated to form plate-like crystals at the tips of ice needles. By the time heating is switched off in the syntheses described in Sections 2.1–2.3, these nanorods have mostly redissolved into solution. However, in the synthesis described in Section 2.4, these nanorods instead persist and thicken as shown in Supplementary Figure S1A. During this synthesis, nanoplates frequently become separated from the thickened nanorods, often leaving the nanoplate with a central nanopore as seen in Supplementary Figure S1B. These nanopores are typically circular and range from 20 to 25 nm in diameter.

## 4 Conclusion

In this study, we have demonstrated a viable chemical route to the formation of moiré materials based on multilayer 2D chalcogenides by leveraging screw dislocation-driven growth. We

observed twist angles up to  $0.52^\circ$  utilizing high-resolution microscopy and simulation. We suggest that the presence of moiré patterns in  $\text{Sb}_2\text{Te}_3$  spiral-type nanoplates is due to increased strain within the central screw dislocation, and that this strain has been modulated by changes to the rate and method of  $\text{N}_2\text{H}_4$  addition during synthesis. Further exploration may lead to precise chemical control over the resulting twist angle. Given that the syntheses put forward in this study are simple and scalable, we believe that this approach to moiré patterns in spiral-type  $\text{Sb}_2\text{Te}_3$  nanoplates could represent an exciting new way to create twistrionic systems, ready for use in electronic devices.

## Data availability statement

The raw data supporting the conclusion of this article will be made available by the authors, without undue reservation.

## Author contributions

RL wrote the manuscript, performed computations, and created the figures. RL and GM developed synthesis methods. DC coordinated the project. All authors have discussed the results, contributed to manuscript revision, and have approved the submitted version.

## Funding

The Carroll lab was provided by Streamline Automation: U.S. Department of Defense/Air Force under Grant No. GR-00000327.

## Acknowledgments

We would like to thank Martin Guthold and Stephen Baker for allowing us access to their equipment and for their work gathering AFM data.

## Conflict of interest

The authors declare that the research was conducted in the absence of any commercial or financial relationships that could be construed as a potential conflict of interest.

## Publisher's note

All claims expressed in this article are solely those of the authors and do not necessarily represent those of their affiliated

organizations, or those of the publisher, the editors and the reviewers. Any product that may be evaluated in this article, or claim that may be made by its manufacturer, is not guaranteed or endorsed by the publisher.

## Supplementary material

The Supplementary Material for this article can be found online at: <https://www.frontiersin.org/articles/10.3389/fmats.2022.963775/full#supplementary-material>

## References

- Cao, Y., Fatemi, V., Demir, A., Fang, S., Tomarken, S. L., Luo, J. Y., et al. (2018). Correlated insulator behaviour at half-filling in magic-angle graphene superlattices. *Nature* 556 (7699), 80–84. doi:10.1038/nature26154
- Cao, Y., Fatemi, V., Fang, S., Watanabe, K., Taniguchi, T., Kaxiras, E., et al. (2018). Unconventional superconductivity in magic-angle graphene superlattices. *Nature* 556 (7699), 43–50. doi:10.1038/nature26160
- Chen, L., Liu, B., Abbas, A. N., Ma, Y., Fang, X., Liu, Y., et al. (2014). Screw-dislocation-driven growth of two-dimensional few-layer and pyramid-like  $\text{WSe}_2$  by sulfur-assisted chemical vapor deposition. *ACS Nano* 8 (11), 11543–11551. doi:10.1021/nn504775f
- Dun, C., Hewitt, C. A., Li, Q., Xu, J., Schall, D. C., Lee, H., et al. (2017). 2D chalcogenide nanoplate Assemblies for thermoelectric applications. *Adv. Mat.* 29 (21), 1700070. doi:10.1002/adma.201700070
- He, F., Zhou, Y., Ye, Z., Cho, S. H., Jeong, J., Meng, X., et al. (2021). Moiré patterns in 2D materials: A review. *ACS Nano* 15 (4), 5944–5958. doi:10.1021/acsnano.0c10435
- Hennighausen, Z., Lane, C., Buda, I. G., Mathur, V. K., Bansil, A., and Kar, S. (2019). Evidence of a purely electronic two-dimensional lattice at the interface of TMD/ $\text{Bi}_2\text{Se}_3$  heterostructures. *Nanoscale* 11 (34), 15929–15938. doi:10.1039/C9NR04412D
- Lau, C. N., Bockrath, M. W., Mak, K. F., and Zhang, F. (2022). Reproducibility in the fabrication and physics of moiré materials. *Nature* 602 (7895), 41–50. doi:10.1038/s41586-021-04173-z
- Li, H., Li, S., Regan, E. C., Wang, D., Zhao, W., Kahn, S., et al. (2021). Imaging two-dimensional generalized Wigner crystals. *Nature* 597 (7878), 650–654. doi:10.1038/s41586-021-03874-9
- Libbrecht, K. G. (2005). The physics of snow crystals. *Rep. Prog. Phys.* 68 (4), 855–895. doi:10.1088/0034-4885/68/4/R03
- Liu, J., Huang, Q., Qian, Y., Huang, Z., Lai, F., Lin, L., et al. (2016). Screw dislocation-driven growth of the layered spiral-type SnSe nanoplates. *Cryst. Growth & Des.* 16 (4), 2052–2056. doi:10.1021/acs.cgd.5b01708
- Liu, L., Sun, Y., Cui, X., Qi, K., He, X., Bao, Q., et al. (2019). Bottom-up growth of homogeneous Moiré superlattices in bismuth oxychloride spiral nanosheets. *Nat. Commun.* 10 (1), 4472. doi:10.1038/s41467-019-12347-7
- Morin, S. A., Forticaux, A., Bierman, M. J., and Jin, S. (2011). Screw dislocation-driven growth of two-dimensional nanoplates. *Nano Lett.* 11 (10), 4449–4455. doi:10.1021/nl202689m
- Zhuang, A., Li, J., Wang, Y., Wen, X., Lin, Y., Xiang, B., et al. (2014). Screw-dislocation-driven bidirectional spiral growth of  $\text{Bi}_2\text{Se}_3$  nanoplates. *Angew. Chem. Int. Ed.* 53 (25), 6425–6429. doi:10.1002/anie.201403530